R_{cp} for charged high p_T pions in $d-Au$ collisions at $\sqrt{s_{NN}} = 200$ GeV

Jiangyong Jia,Brian Cole

July 11, 2004

Abstract

We presents the details on extracting $\pi^{\pm}$ yield in $d-Au$ collisions at $\sqrt{s_{NN}} = 200$ GeV/c. High momentum $\pi^{\pm}$ ($p > 4.7$ GeV/c) are identified using RICH and EMCal detectors. One of the crucial problems is to estimate the $e^{\pm}$ from conversion which may also satisfy our RICH and EMCal cuts. From the background free pion raw spectra, we obtain central to peripheral ratio R_{cp}.

Contents

1 Introduction

It was shown before that charged pions with momentum $\gtrsim 4.7$ GeV/c fires PHENIX RICH detector [1, 3, 4]. The typical variable used to quantify the RICH response for charged particles is N_{PMT} - number of photo multiplier tubes fired at RICH. As shown in Fig. 1, the mean number of PMTs quickly increases below 8 GeV/c, but only increases slowly after 8 GeV/c. The actually detection efficiency depends on the threshold of N_{PMT} cut. As Fig. 2 shows (close circle), for the RICH cut used in this study, $N_{PMT} > 0$, the pion efficiency quickly rises and become $> 90\%$ at $p_T > 6$ GeV/c. For stronger cut,$N_{PMT} \geq 5$, the efficiency has a much flatter turn on region and saturates at around $\approx 50\%$ at $p_T = 20$ GeV/c.

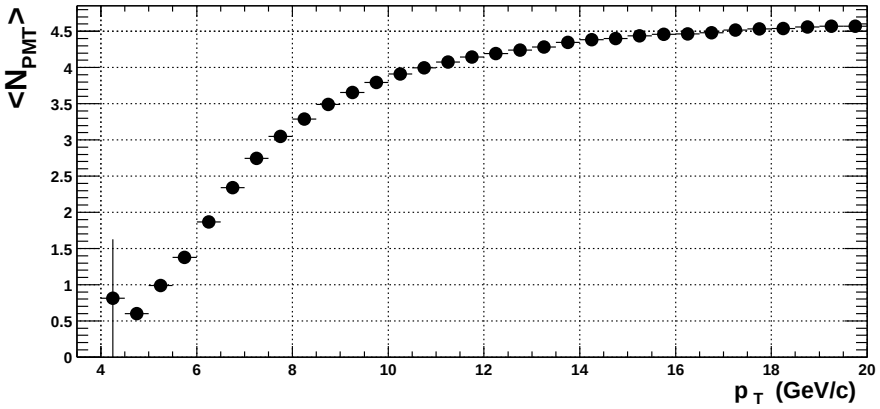

Figure 1: The $\langle N_{PMT} \rangle$ as function of p_T for $\pi^+ + \pi^-$ from simulation.

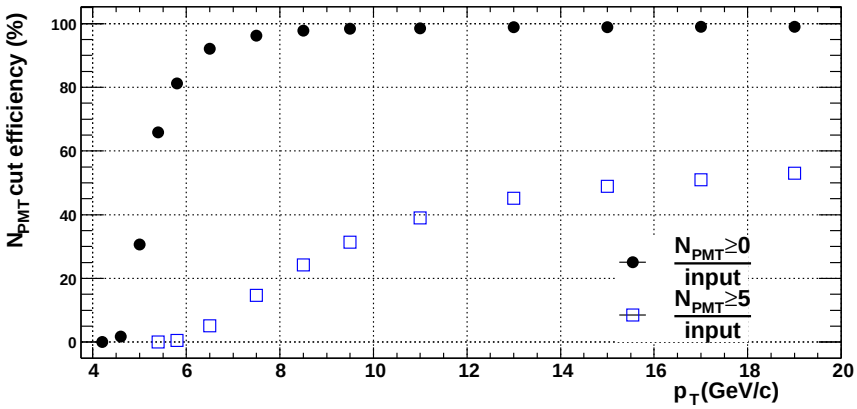

Figure 2: RICH efficiency in the active detector region for $\pi^+ + \pi^-$ as function of p_T from simulation. The close circles represent efficiency for $N_{PMT} > 0$ cut and the open boxes represent efficiency for $N_{PMT} \geq 5$ cut.

Table 1: The three datasets used in this analysis and corresponding pion statistics.

	Minimum bias	ERT electron trigger	ERT photon trigger
evts(M)	87.14	95.27	48.51
sampled evts(M)	87.14	4359.5	≈ 5000
pions candidates	1651	38280	39627

2 Event and centrality selection

We have used three types of trigged data in current study, and we applies a 30 cm cut on the collisions bbcz-vertex.(In principle, this vertex can be relaxed to gain more statistics.) The statistics for three triggered datasets and corresponding number of high p_T pions candidates for the cut we used in this analysis are listed in Table. 1, the distributions of the number of high p_T pion candidates for CNT_Minbias, CNT_Electron and CNT_Photon are shown in Fig. 3. We have a total of 486 runs. As a reminder, the pion candidates we are talking here were selected with somewhat less stringent cut than those used to make the final R_{cp} plot.

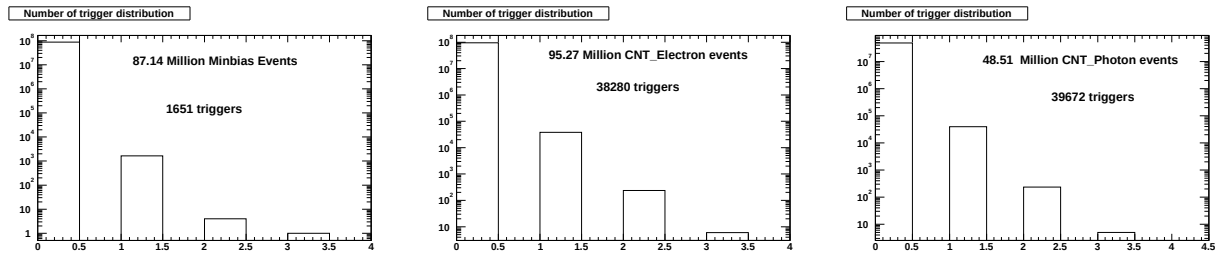

Figure 3: Total number of trigger particle distribution for CNT_Minbias (left) CNT_Electron(center) and CNT_Photon(right). The total integral of each histogram represent their total events on disk.

Fig.4 shows the centrality and vertex distribution of the minimum bias events. The event centrality is calculated from the south BBC hits distribution which is detailed in analysis note 210 [5].

To study the nuclear modification factor R_{dAu} or R_{cp}, one need to know the N_{coll} for each centrality bin. We use the numbers documented in analysis note 210 [5], they are listed in Table. 2.

2.1 Data quality check

For charged pion spectra, we uses only events that fired electron triggers. Detailed RUN3 ERT trigger performance can be found in [2]. According to this note, ERT trigger becomes stable after RUN71723. So we exclude the earlier runs for the R_{cp} analysis. Fig. 5 shows the high p_T pion candidate statistics for those runs. In total, we rejected 3151 pions in 127 runs, which corresponds to about 8% of all pions statistics.

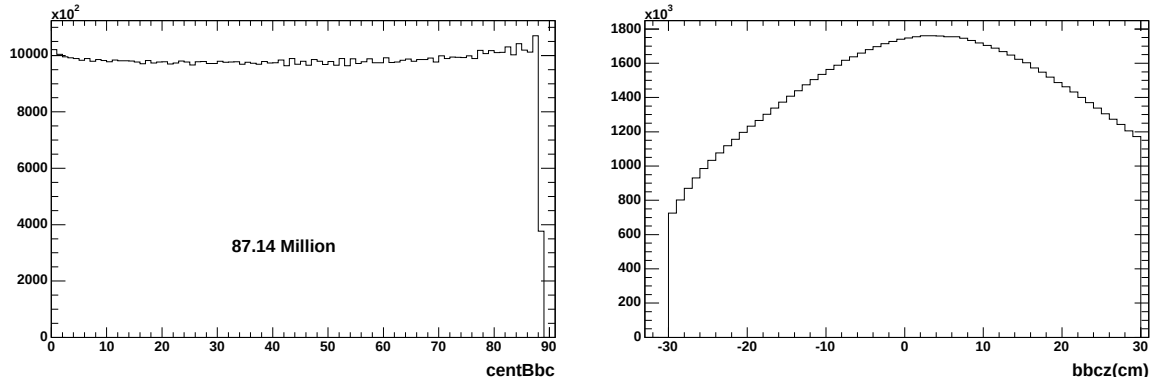

Figure 4: The centrality(left) distribution and bbc zvertex(right) distributions for Minimum bias distributions.

centrality	$\langle N_{coll} \rangle$	Ratio to most peripheral class	Bias correction
0-88	8.5 ± 0.4	-	> 0.99
0-20	15 ± 1	4.6 ± 0.5	> 0.99
20-40	10.4 ± 1.7	3.2 ± 0.2	> 0.99
40-60	6.9 ± 0.6	2.1 ± 0.1	0.974 ± 0.01
60-88	3.2 ± 0.3	1.0	0.885 ± 0.04

Table 2: $\langle N_{coll} \rangle$ and it errors and BBC trigger bias (see following discussion) for minimum bias collisions and the four centrality classes used in this analysis.[5]

In RUN3, the Level-1 electron trigger threshold was set at 0.8 GeV with 2×2 tiles. With this threshold the trigger rejection is about 20-30, and no prescale is needed is most of the running period. Run 76851, 77531, 77678, 78306 are the only one that were pre-scaled by 2, we need to divided the sampled MB events by 2 for those runs in order to have proper normalization.

To minimize the run-by-run variation, we rejects those runs with less than 16 pion candidates in them. This rejects a total of 382 triggers in 53 runs. Fig. 6 shows the number of sampled minimum bias event per high p_T pion as function of run number for runs with more than 16 high p_T pion candidates. Roughly, for **every 100k** minimum bias events, there is **one** high p_T pion candidate passing the offline cut. As a quality control, we exclude runs that have too much or too less pion candidates. The cut on sampled events per pion candidate is indicated by the horizontal lines. Three runs, 76274(261 triggers), 74660(41 triggers),78402(36 triggers), are excluded. These runs might have different energy threshold or different trigger pedestals.

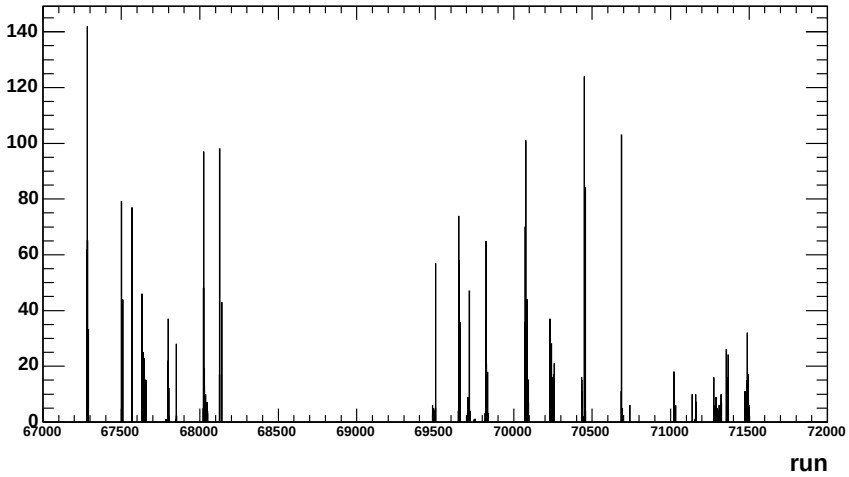

Figure 5: Runs excluded for the spectra analysis due to problems in the ERT trigger according to [2].

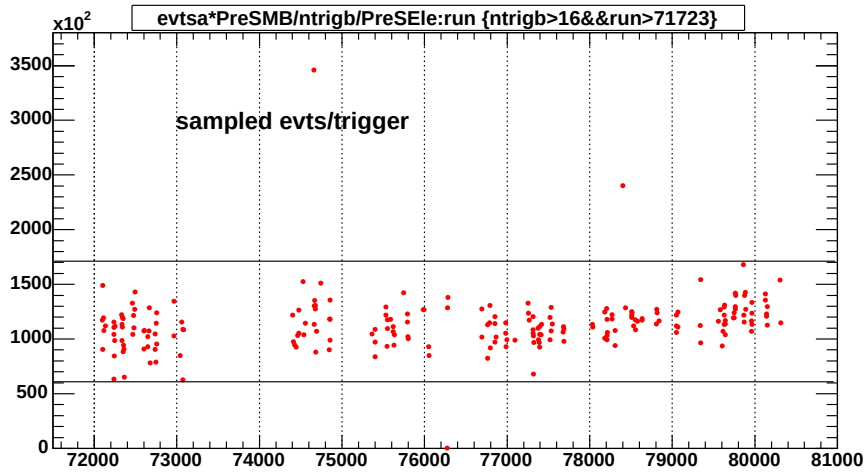

Figure 6: Number of sampled minimum bias events per high p_T pion vs run number for runs with more than 16 pions. Good runs are between the horizontal lines.

3 Backgrounds

3.1 Background sources

RICH Cherenkov threshold for charged particles is $\gamma \approx 35$, which is 0.017, 3.5 and 4.7 GeV/c for electron, muon and pion respectively. Typical e/π or μ/π ratios for primary electron and muons are less than 10^{-3}. Fig. 7 shows the raw yields vs p_T in minimum bias events for all tracks with 3 σ association at PC3 and $N_{PMT} \geq 0$. Already with this very loss cut, one can see a bump around 5-6 GeV/c, indicative of the turn on of pion signal. There are two main

sources contributing to the backgrounds in Fig. 7.

1. conversion electrons generated in front of or inside the X1 layer of the DC. These electrons fires RICH and frequently are also reconstructed with a large momentum (See [4, 3]).

2. Decay background or primary charged particles which do not fire the RICH, but are randomly associated with a RICH ring.

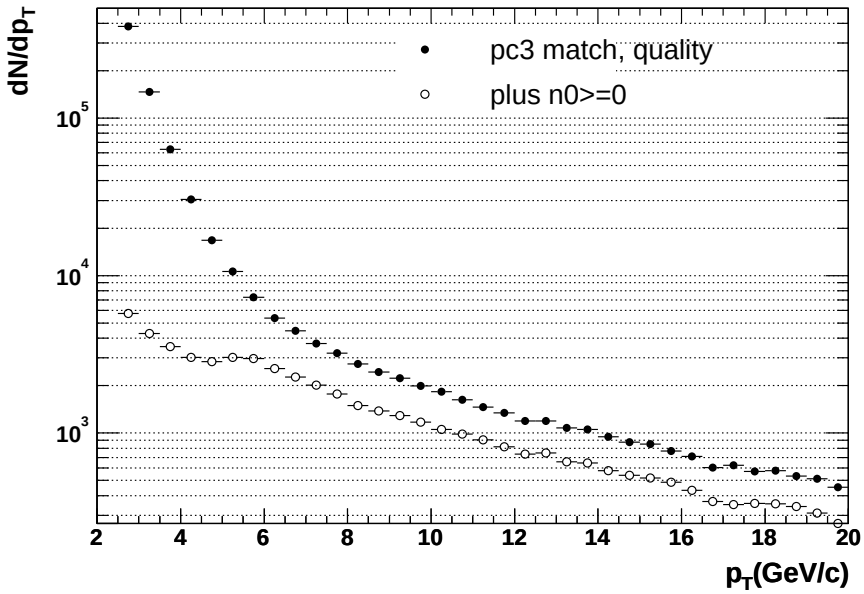

Figure 7: Effect of requiring $N_{PMT} \geq 0$ for minimum bias collisions. The p_T distribution for charged tracks satisfying 3σ matching cut at PC3 and quality cut in the DC (31 or 63) is indicated by the solid circles; The p_T distribution with additional confirmation hit at RICH is indicated by the open circles.

The random association probability depends only on the detector occupancy, and can be very well studied using the swap variables in the nanodst. Please refer to [4] for detailed discussion on the estimation of occupancy effects. Unfortunately, the swap variables were not filled in RUN3 nanoDSTs. Instead, we estimated the occupancy effect using RUN2 peripheral $Au - Au$ data(Section.4.1). The random association probability at RICH is about 0.4%.

The conversion background requires somewhat more sophisticated approached to estimate and subtract. First, the conversion backgrounds in our analysis are generated mostly in front of the DC, the actual background as function of p_T is the result of the detailed convolution of parent γ distribution, conversion kinematics and the material distribution. Secondly, the energy deposition and shower shape for conversion electrons and pions in Emcal are very different. Electrons deposit 100% of their energy in Emcal and the shower energy is usually contained in a few towers. On the other hand, hadrons typically deposit a fraction of their total energy, but with a much broader shower shape.

In analysis note 177, we found that the both type of backgrounds have strong zed dependence. We found similar effect in $d-Au$ as shown in Fig. 8. The left panel shows the zed dependence for tracks with reconstructed $p_T > 5$ GeV/c plotted for conversion contaminated sample (solid line), decay contaminated sample(dotted line) and conversion contaminated sample with a p_T dependent energy cut. There are more tracks at high zed for conversion contaminated sample indicting there are more conversion background at large zed. Similar trend is seen for the decay contaminated sample with weaker zed dependence. The reason for this zed dependence is due to the zed dependence of the residual bend as argued in Analysis note 177 [3]. Because the residual field decreases towards large zed, there are more background tracks surviving the 3σ PC3 matching cut at large zed than at small zed. Obviously, the zed dependence become weaker after one applies an energy cut.

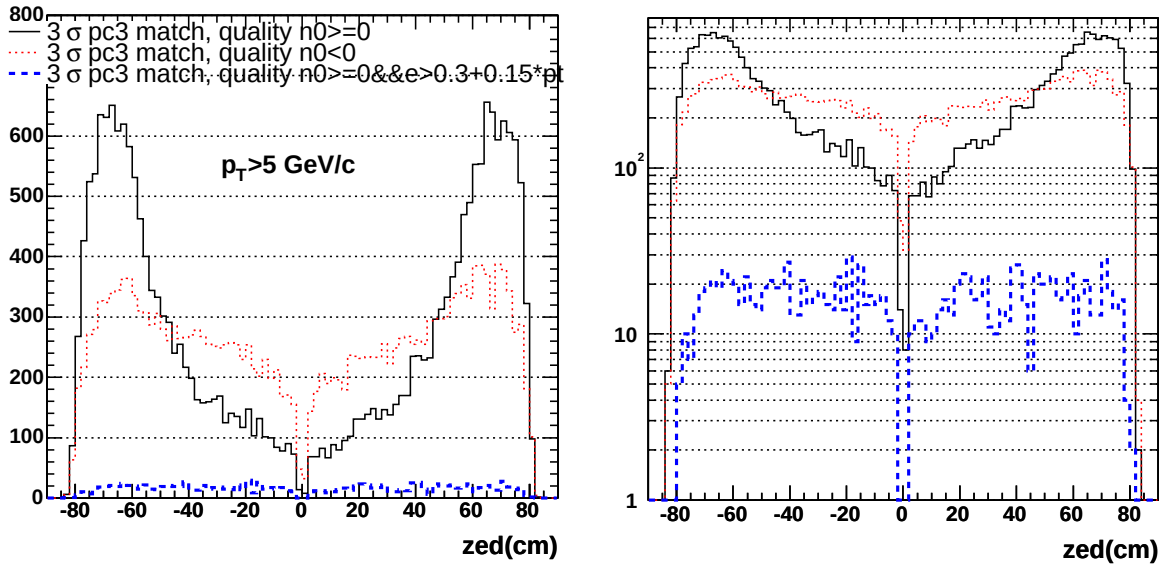

Figure 8: The zed dependence for tracks with reconstructed $p_T > 5$ GeV/c plotted for conversion contaminated sample (solid line), decay contaminated sample(dotted line) and conversion contaminated sample with a p_T dependent energy cut. the right figure shows the same set of histograms on log scale for better view.

3.2 Response in RICH

From RUN2 charge hadron analysis, we also know that the RICH response for charged particles also have a zed dependence [4, 3], which was also confirmed in Monte-carlo simulation. In order to study the RICH responds for electrons, we follow a procedure similar to the one used in [4]. A pure sample of conversion electrons are selected by requiring an energy cut of $e > 0.5$ GeV in EMCal and matching cut of $5\sigma > |pc3sd\phi| > 3\sigma$ at PC3. This cut basically selects soft conversion electrons which were deflected into $5\sigma > |pc3sd\phi| > 3\sigma$ either from multiple scattering or bend by the residual magnetic field [1]. Then the zed dependence of

[1]Note that we didn't use RICH detector in this selection.

RICH responds is studied from this sample of conversion electrons. Fig. 9 shows the zed dependence of the N_{PMT} cut efficiency for the conversion electrons selected for CNT_Minbias events. Five different N_{PMT} cuts are used and the ratio of the four cuts to the weakest cut are plotted. Clearly, one notices a dropping trend of the ratio at large zed. This indicates that the average associated N_{PMT}s per electron or the efficiency decrease as zed increases. The line on each of the four ratios represent a liner fit with the fitted parameters shown in the legend. The liner fits work well in describing the zed dependence. [2].

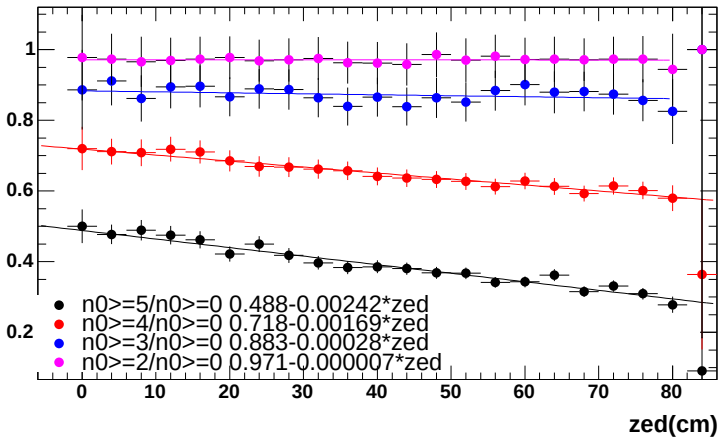

Figure 9: Zed dependence of N_{PMT} cut efficiency for the conversion electrons selected for CNT_Minbias events. Five different N_{PMT} cuts are used and the ratio of the four cuts to the weakest cut are plotted. The lines represent linear fits on the ratios, the fitted values are also shown in the figure.

3.3 Response in EMcal

To reject the conversion backgrounds at high p_T, one have to rely on EMCal cuts. The relevant variables are:

1. *ecore* : the core energy of the shower under the assumption that it is electromagnetic.
2. *e*: The total energy summed over all connected towers with energy greater than 30 MeV(from Sasha).
3. *emcchi*2: The variable used to characterize the "photonness" of a shower [8]. For each shower (cluster) the energy deposit pattern is tested against the known(energy- and impact point-dependent) energy deposit pattern of an electromagnetic shower and χ^2 is calculated.

[2]This efficiency can also be obtained from conversions from convertor or electrons selected using e/p cut. Result is consistent

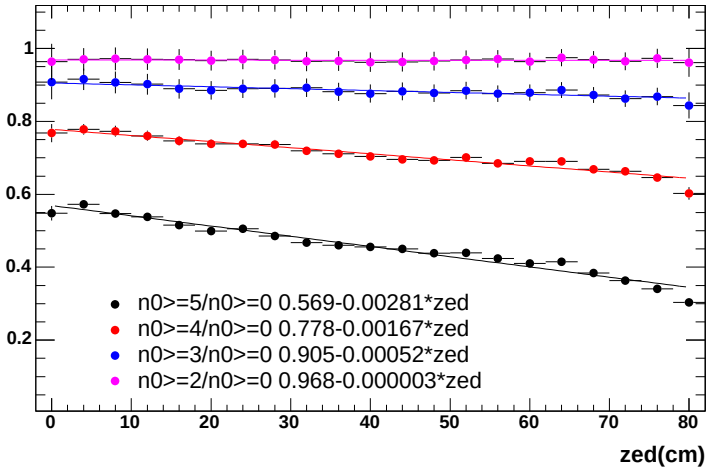

Figure 10: Zed dependence of N_{PMT} cut efficiency for the conversion electrons selected for CNT_Electron events. Five different N_{PMT} cuts are used and the ratio of the four cuts to the weakest cut are plotted. The lines represent linear fits on the ratios, the fitted values are also shown in the figure.

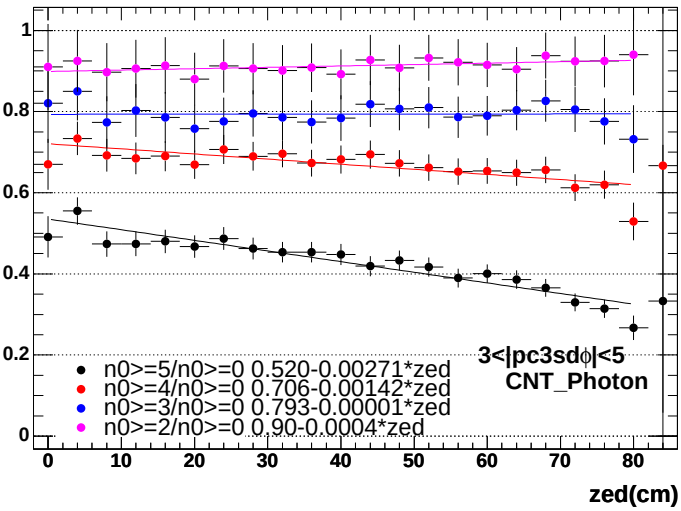

Figure 11: Zed dependence of N_{PMT} cut efficiency for the conversion electrons selected for CNT_Photon events. Five different N_{PMT} cuts are used and the ratio of the four cuts to the weakest cut are plotted. The lines represent linear fits on the ratios, the fitted values are also shown in the figure.

4. *prob_photon*(*prob*): The normalized photon probability from emcchi2. For photon (and electron to some extent). The probability distribution is flat from 0 to 1.

5. *dispy*, *dispz* : The second moment of the tower positions distribution within the cluster along y and z axis.

The most effective cut is the cut on e or $ecore$. In analysis note 127 [1], Federica used $ecore > 0.16 + 0.33 \times p_T$ in $Au - Au$ analysis, as we shall demonstrate later, this cut is too strong for high p_T pions in $d - Au$. And we will demonstrate that in fact a weaker energy cut is sufficient in rejecting the background. Fig. 12 shows the p_T spectra with different energy cuts. Clearly, a constant energy cut will eventually underestimate the background at high enough p_T, and a sliding energy cut is much better in this respect. However, it is also tricky figure out the cut efficiency, but it is ok for making R_{cp}. Of all different cuts, we can see that $e > 0.3 + 0.15 p_T$ gives reasonable spectra spectra shape(so almost background free) while preserving the pion statistics at lower p_T. Since conversion electrons tends to bend due to the residual field, by looking at the shape of the matching distribution, we can judge whether there are background in the spectra. Fig. 13 shows the PC3 matching distribution in ϕ for different energy cuts. This figure qualitatively confirm that $e > 0.3 + 0.15 p_T$ cut removes all of the conversion backgrounds outside the matching window. From now on, we shall make this energy cut our default, and we will later prove that combining this cut with prob cut is enough to reject conversion background out to 15 GeV/c.

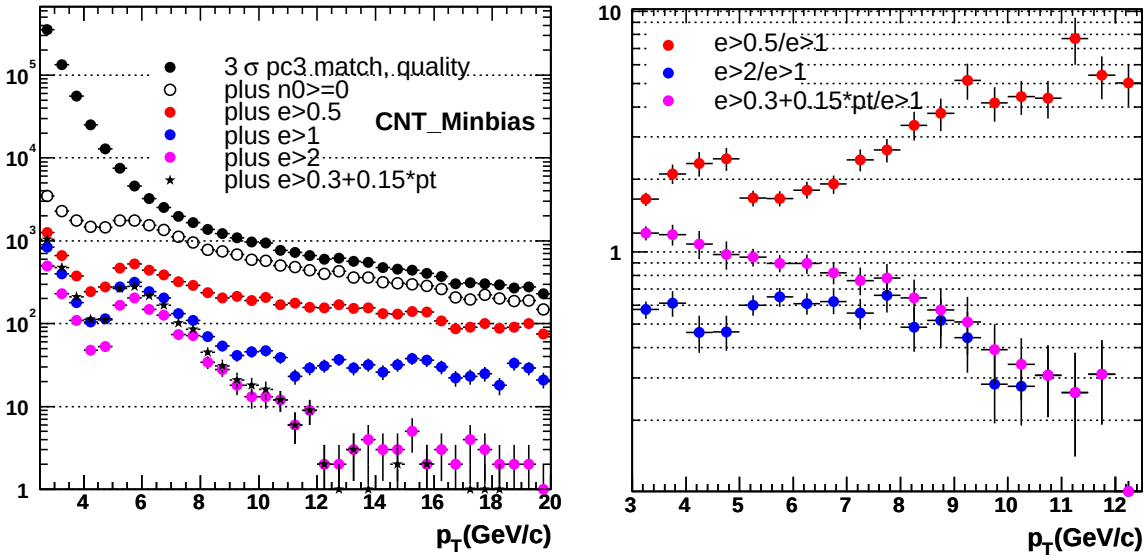

Figure 12: a). The p_T spectra with different energy cut at EMCal. b). The ratios of spectra for various energy cut to that for $e > 1$.

We can very accurately estimate the background contamination in the pion candidates with $5.5 < p_T < 7$ 7 GeV/c. Since pions on average fires a small N_{PMT} (see Fig. 1), we can select a certain fraction of conversion electrons by requiring $N_{PMT} > 4$, then divided it by the cut efficiencies in Fig. 9-11 to estimate the total electron contributions. The result of this study using CNT_Electron is shown in Fig. 14, where one can see that the estimated electron background in the pion candidates is less than 10%. This actually is an upper limit, since there is a small probability for pion to pass $N_{PMT} \geq 5$, thus counted as background, and this probability increases rapidly with p_T.

Since the background contribution can be estimated reliably in 5.5-7 GeV/c using only RICH, we can extract the true pion yield. We can then using these pions to calibrate

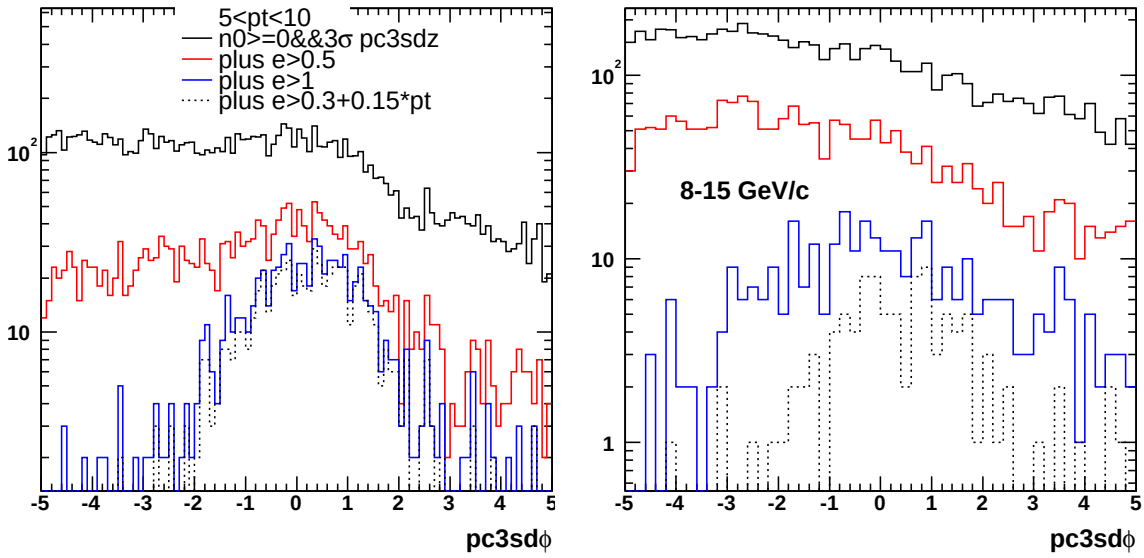

Figure 13: a). The PC3 matching in ϕ direction with four different cuts at EMCal for tracks with reconstructed p_T $5 < p_T < 10$ GeV/c. b). The same distribution but for tracks with reconstructed p_T $8 < p_T < 15$ GeV/c.

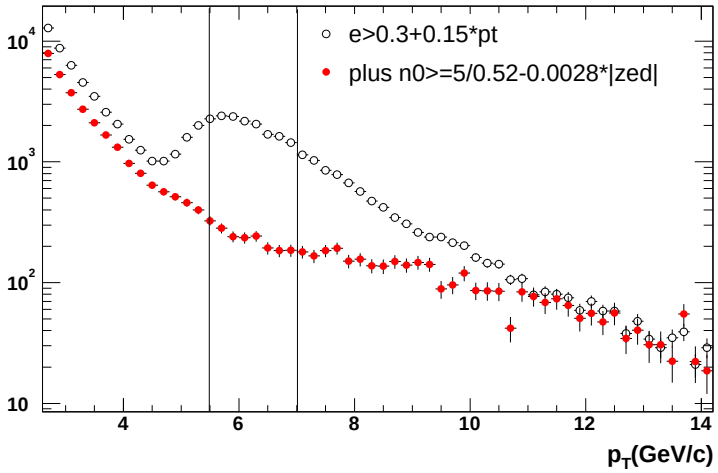

Figure 14: The charged pion candidates distribution(in open symbol) and the estimated background contributions(in solid symbol) for CNT_Electron.

EMCal responds for pions. Fig. 15a shows the e/p and $ecore/p$ distribution for estimated backgrounds and all charged tracks with association in RICH. The peak around $e/p = 1$ is clearly visible, which corresponds to electrons originate at or close to vertex (like conversions at beam pipe). By subtracting electron distribution from the pion distribution, we get pure pion e or $ecore$ distributions, which are shown in Fig. 15b. The integral for $e/p > 0.4$(to the right of the vertical line) is about 27.2% while $ecore/p > 0.4$ is only 17.7%. So variable 'e'

is more suitable for selecting high p_T pions than '*ecore*'.

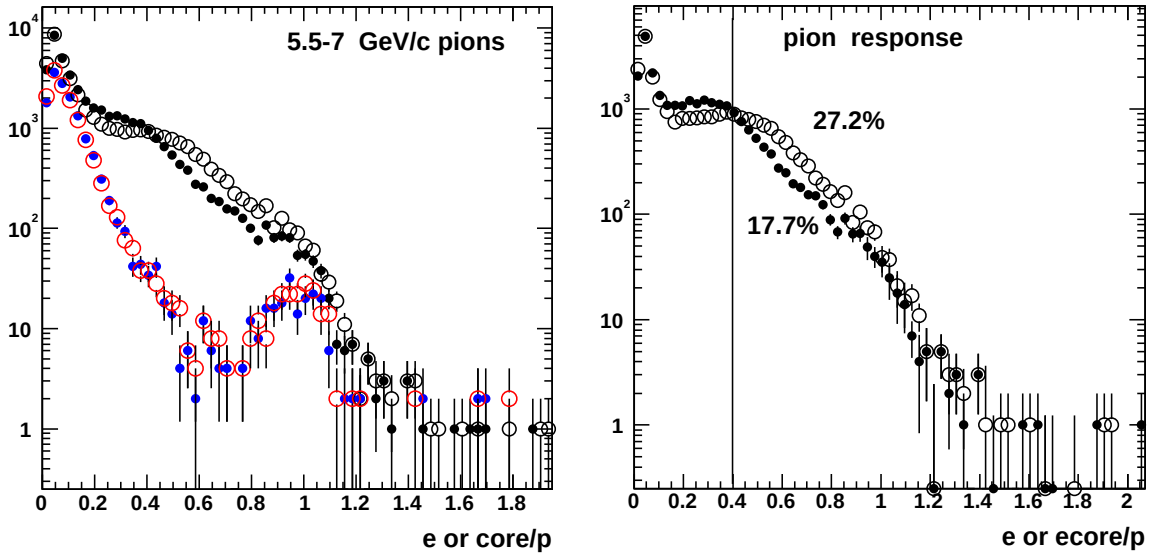

Figure 15: a) The upper two histograms represents pion candidates distributions as function of e/p(open) and $ecore/p$ (solid). The lower two histograms represent electron distributions estimated requiring $N_{PMT} \geq 5/eff$ but plotted as function of e/p(open) and $ecore/p$ (solid), respectively. b) the pion e/p(open marker) and $ecore/p$(solid marker) distribution obtained by subtracting the upper histograms by the lower histograms in the left panels.

The difference of the *prob* distribution for hadrons and photons(electrons) provides additional rejection power on electron backgrounds. The electron *prob* distribution has been heavily studied with test beam data by Sasha [7]. In fact, the *prob* distribution was tuned using test beam electron data to be flat in 0-1. Since we want to use *prob* variable to improve the background rejection, it would be highly desirable to be able to study independently the *prob* distribution using RUN3 data itself. In low p_T region of $2.5 < p_T < 4$, since the charged particles firing RICH should be predominantly electrons, these particles can be used to study the electron *prob* distribution. Fig. 16 shows the e/p distribution for all tracks with $2.5 < p_T < 4$ and $N_{PMT} \geq 0$. The e/p peak around 1 is made of mostly primary electrons or those generated close to the vertex. These electrons are used to study the *prob* distributions.

Fig.17-Fig.19 shows the normalized *prob* distributions for electrons and hadrons in 2.5-4 GeV/c p_T range. The only differences between the three plots are the N_{PMT} cut used to select electrons, i.e. $N_{PMT} \geq 0$ in Fig.17, $N_{PMT} \geq 3$ in Fig.18, and $N_{PMT} \geq 5$ in Fig.19. It is clear from Fig. 16 that higher N_{PMT} cut select more pure electrons, especially in $e/p > 0.75$ regions. By comparing different N_{PMT} and e/p or e cut, we can learn much about the *prob* distribution for pure electrons. In all three figures, the hadron *prob* distribution always peaks at very small value. In fact, about 70% of the hadrons passing corresponding e/p cut have $prob < 0.02$. On the contrary, electron *prob_proton* distribution is almost flat. Except that there is a small peak at small *prob* value when using small e/p cut or N_{PMT} cut, the peak comes from hadrons that have randomly associated RICH hits. As one moves to larger e/p

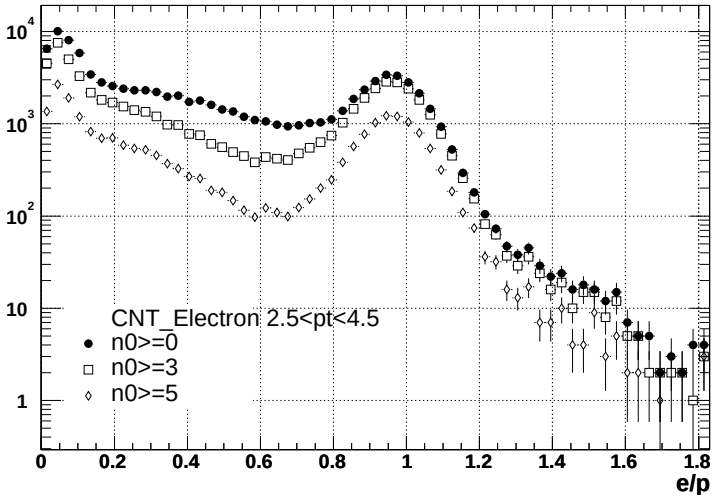

Figure 16: e/p distribution for tracks within 2.5-4 GeV/c, and satieqsfying 3 σ PC3 match and with $N_{PMT} \geq 0$ (solid circles), $N_{PMT} \geq 3$(open boxes) and $N_{PMT} \geq 5$(open diamonds). CNT_Electron is used for this study.

or N_{PMT} cut, this peaks goes away. Comparing closely the three *prob* distributions for

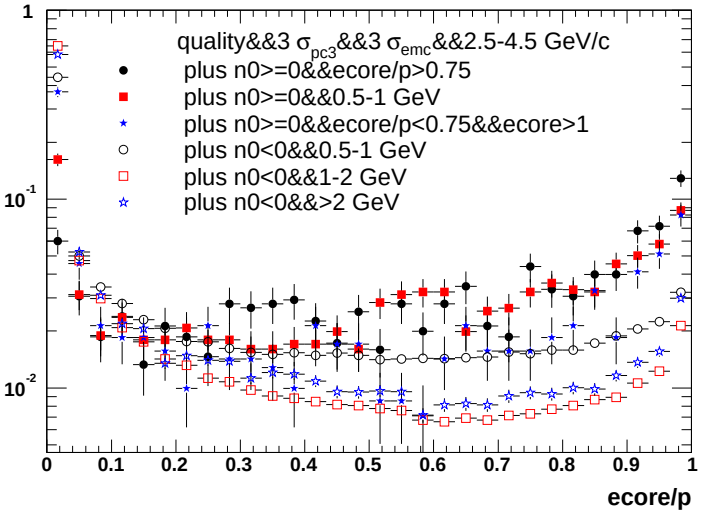

Figure 17: *prob* distributions for hadrons (solid markers) and electron candidates(open markers) with three different e/p cuts. All tracks are between 2.5 to 4.5 GeV/c in p_T, and pass DC quality cut and 3σ matching cut at PC3 and EMCal. Hadron and electron candidates are distinguished by $N_{PMT} < 0$ and $N_{PMT} \geq 0$, respectively. All six histograms are normalized such that the total integral is 1.

hadron in each of the three figures, we noticed that there is a weak dependence of the *prob* distribution on the energy cut at $p_T < 1$ GeV/c. This probably is related to the fact that at small energy, particles with energy around MIP can be miss-identified as photons. From the

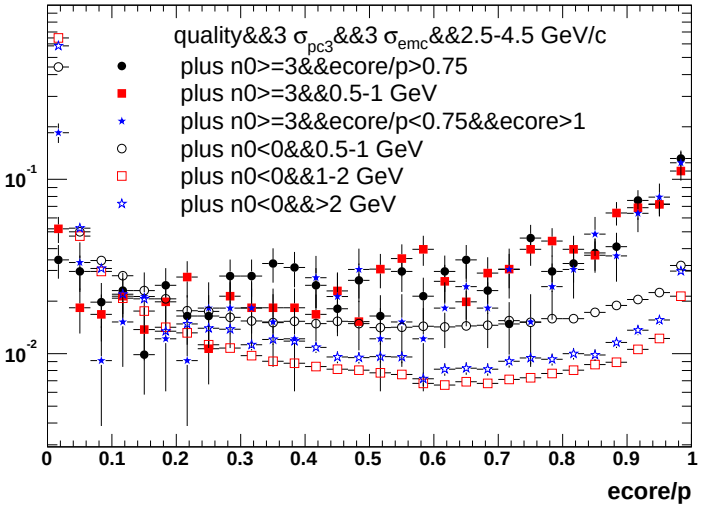

Figure 18: Same as previous plot, except that we apply $N_{PMT} \geq 3$ on electron candidates. Compare with Fig.16 to have a feeling on the purity of the electron sample.

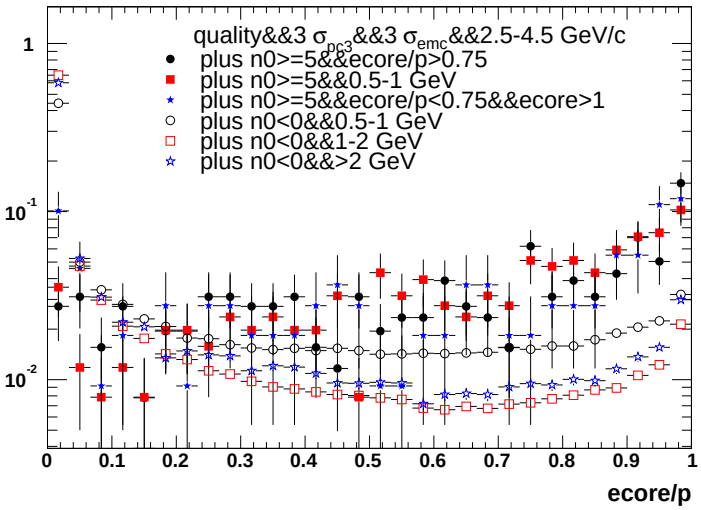

Figure 19: Same as previous plot, except that we apply $N_{PMT} \geq 5$ on electron candidates. Compare with Fig.16 to have a feeling on the purity of the electron sample.

three figures, we can roughly estimate the cut efficiency with *prob*. The estimated efficiencies are listed in Table. 3. The efficiency is about 90% with $prob < 0.2$ and decrease to 70% with $prob < 0.02$. In order to keep relative high efficiency for hadrons, we shall use $prob < 0.2$ for the final R_{cp} analysis.

The effects of *prob* cut for CNT_Electron are shown in Fig. 20. In the left panel, pion spectra with four different *prob* cut, $prob < 0.4$(open boxes), $prob < 0.2$(open diamonds), $prob < 0.1$(solid stars) and $prob < 0.05$(crosses) are shown together with the one without *prob* cut(solid circles). In the right panel, we shows the spectra for particles that are successively

$prob$	< 0.2	< 0.1	< 0.05	< 0.02
effi	0.9	0.84	0.8	0.7

Table 3: The $prob$ cut efficiency for hadron tracks with $2.5 < p_T < 4$ and $e > 1$ GeV.

cut away by the four cuts, $prob > 0.4$(open boxes), $0.2 < prob < 0.4$(open diamonds), $0.1 < prob < 0.2$(solid stars) and $0.05 < prob < 0.1$(crosses). It is clear that $prob < 0.4$ removes about 10-20% of pions, but most of the stuff it removes are conversion backgrounds. Going from $prob < 0.4$ to $prob < 0.2$, the amount of rejected background and signal are almost comparable. Any $prob$ cuts below 0.2 cuts away more signal than background(because the background is already very tiny). The effect of $prob$ cut for the case where there is already an EMCal energy cut of $e > 1$ GeV is shown in Fig. 21. Clearly, below 8 GeV/c, there is no gaining by applying both the energy and $prob$ cut. In fact, at $p_T < 8$, requiring $e > 1$ GeV/c cuts away 20% more pion.

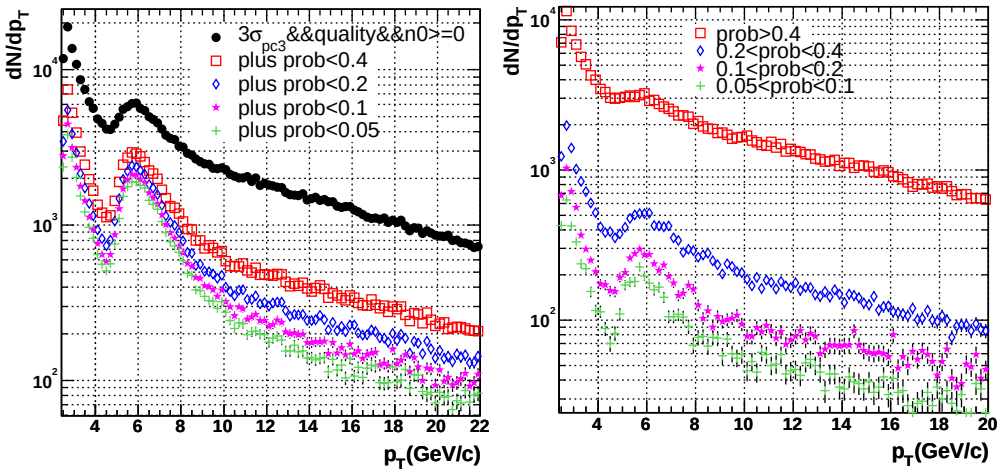

Figure 20: a). Raw pion spectra from CNT_Electron with four different $prob$ cut, $prob < 0.4$(open boxes), $prob < 0.2$(open diamonds), $prob < 0.1$(solid stars) and $prob < 0.05$(crosses) are shown together with the one without $prob$ cut(solid circles). b). The raw spectra for particles that are successively cut away by the four cuts, $prob > 0.4$(open boxes), $0.2 < prob < 0.4$(open diamonds), $0.1 < prob < 0.2$(solid stars) and $0.05 < prob < 0.1$(crosses).

We repeat the same study for minimum bias events, the results are shown in Fig. 22 and Fig. 23. The statistic in this case is poor, but minimum bias data allows us to directly calculate the efficiency of the cuts. we can roughly read from the figure that the efficiency for $prob < 0.4$ cut is about 75%. On the other hand, by comparing the histograms with and without energy cut(comparing the histograms indicated by solid circles in Fig. 22 with the one in Fig. 23), we conclude that an energy cut of $e > 1$ GeV/c leads to about 40% pion efficiency loss at around 6 GeV/c.

The amount of remaining conversion background around 6 GeV/c with both $prob$ cut($prob < 0.2$) and energy cut($e > 1$ GeV/c) is very small, mostly likely $< 5\%$(this can be easily

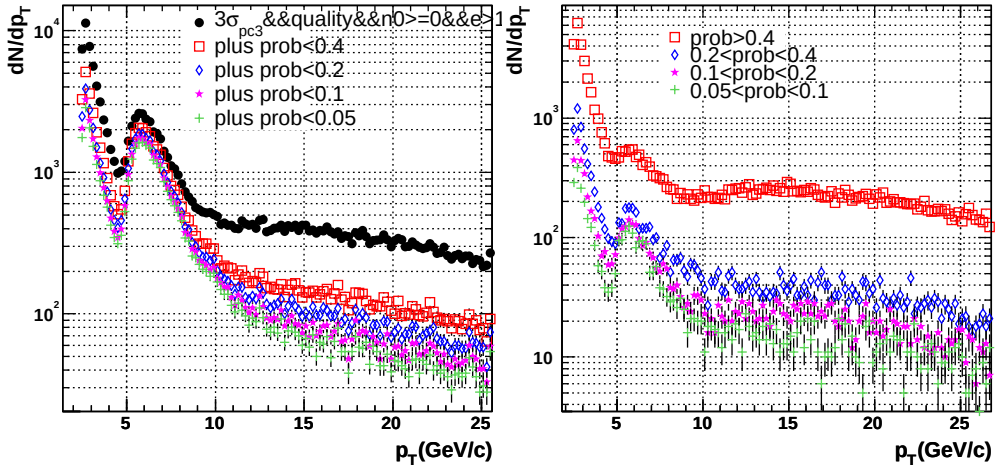

Figure 21: Same condition as previous figure, except that we require in addition a 1 GeV energy cut: $e > 1$ GeV.

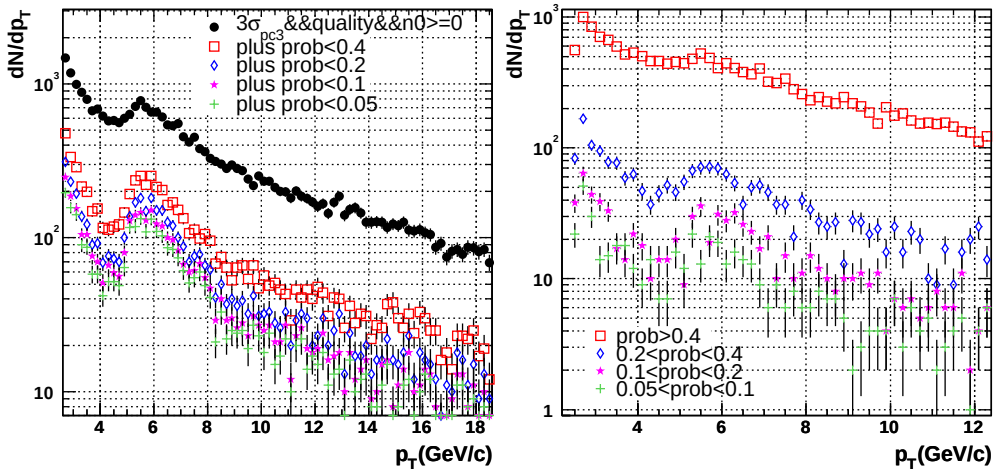

Figure 22: a). Raw pion spectra from CNT_Minbias with four different *prob* cut, $prob < 0.4$(open boxes), $prob < 0.2$(open diamonds), $prob < 0.1$(solid stars) and $prob < 0.05$(crosses) are shown together with the one without *prob* cut(solid circles). b). The raw spectra for particles that are successively cut away by the four cuts, $prob > 0.4$(open boxes), $0.2 < prob < 0.4$(open diamonds), $0.1 < prob < 0.2$(solid stars) and $0.05 < prob < 0.1$(crosses).

checked by extrapolating the background < 4.5 GeV/c). Fig. 24 shows the raw spectra by combining a fixed *prob* cut($prob < 0.2$) and different sliding the energy cut, Since the energy cut and *prob* cut is orthogonal to each other, the fact that the ratio between solid blue and magenta curve is approximately constant(look by eye), indicate that the energy cut of $e > 0.3 + 0.15pt\&\&prob < 0.2$ is enough to reject backgrounds up to 16 GeV/c.

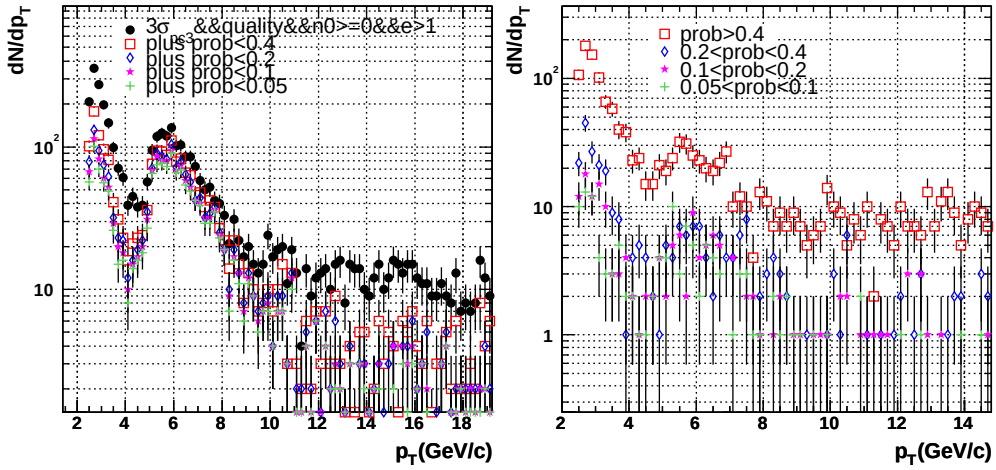

Figure 23: Same condition as in previous figure, except that we require in addition a 1 GeV energy cut: $e > 1$ GeV.

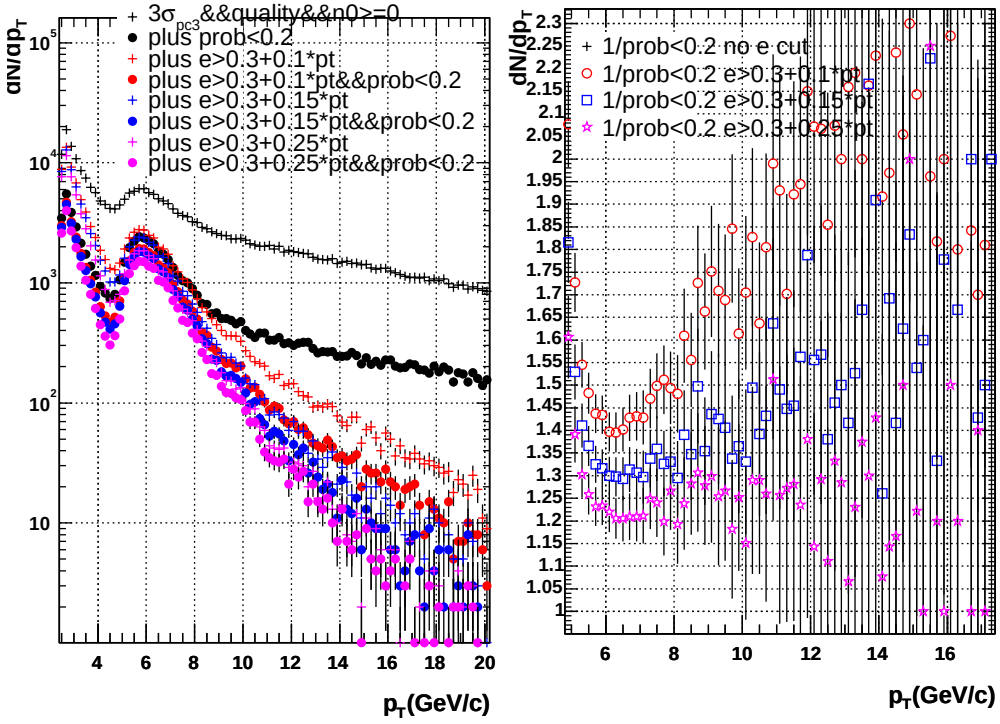

Figure 24: a). Raw spectra using varying energy cut only(cross marker) or plus prob cuts (solid marker). b). The ratios between the raw spectra without energy and prob cut to the ones with $prob < 0.2$ and different sliding energy cut.

4 Measurement of R_{cp}

The cuts developed in previous section allow us to remove most of the background in the pion spectra. However, it is very difficult to know the pion efficiency associated with those cuts, so we are not yet ready to extract the absolutely corrected p_T spectra. But it is straight forward to produce the charged pion R_{cp}. The assumption is that the trigger efficiency, trigger bias and offline cuts have no centrality dependence.

The list of centrality dependent biases and efficiencies are listed as the following,

1. Error on N_{coll} and BBC trigger bias. This has been studied in Analysis note 210 [5].
2. Random association at DC, PC3, RICH and EMCal.
3. Occupancy correction at DC, PC3, RICH, EMCal.
4. Random benefit in Electron triggered events.
5. Single high pt pion efficiency in Electron trigger events.

The main sources at high p_T comes from the BBC trigger bias and the occupancy effect. Once know the pion detection efficiency in offline ϵ_{off} and track by track pion Level-1 trigger efficiency ϵ_1, we can obtain the true pion yield from the raw yield $(dN/dp_T)_{raw}$ as,

$$dN/dp_T = \frac{(dN/dp_T)_{raw}}{\epsilon_{off} \times \epsilon_1} \tag{1}$$

If we are interested only in making R_{cp}, most of the offline reconstruction efficiency and Level-1 trigger cancels, and thus we don't need the absolutely efficiency corrected spectra for making R_{cp}. The centrality dependence of the ϵ_{off} comes mainly from the random background under the offline cuts which might depends on the detector occupancy. The centrality dependence of ϵ_1, on the other hands, comes mainly from trigger random benefit and possible centrality dependence of the trigger threshold due to occupancy effect. In what follows, we shall discuss the offline and Level-1 efficiency separately.

4.1 Random association background

Since $d-Au$ nanoDST does not contain swapped variables, we can't estimate the occupancy effect from $d-Au$ directly. However, based on the fact that the high p_T hadron yield almost scales with N_{ncoll} in peripheral $Au-Au$ [9, 10] and centrality selected $d-Au$ [11, 5] collisions. We can simply assume that the detector occupancy scales with N_{coll}, and uses the peripheral $Au-Au$ data with similar multiplicity as that in $d-Au$ collisions to estimate the occupancy effect. The most central $d-Au$ has $N_{coll} = 15.1$, which corresponds to about 70% centrality bin in $Au-Au$ collisions. In current analysis, we need to estimate the occupancy effects for all tracking detectors used in the analysis. The main sources of random backgrounds include the random match at PC3, EMCal, random association of RICH hits, random smearing of EMCal cluster energy and *prob*. The amount of random for each variable shall be estimated from it's swap variable as function of p_T. The signal and each of the random background contributions in our study is estimated as:

Signal

$|pc3sd\phi| < 3\&\&|pc3sdz| < 3\&\&|emcsd\phi| < 3\&\&|emcsdz| < 3\&\&$
$N_{PMT} \geq 0\&\&e > 0.3 + 0.15p_T\&\&prob < 0.2$

random match at PC3

$|spc3sd\phi| < 3\&\&|spc3sdz| < 3\&\&|emcsd\phi| < 3\&\&|emcsdz| < 3\&\&$
$N_{PMT} \geq 0\&\&e > 0.3 + 0.15p_T\&\&prob < 0.2$

random match at EMC

$|pc3sd\phi| < 3\&\&|pc3sdz| < 3\&\&|semcsd\phi| < 3\&\&|semcsdz| < 3\&\&$
$(|emcsd\phi| > 3||emcsdz| > 3)\&\&N_{PMT} \geq 0\&\&e < 0.3 + 0.15p_T\&\&(e + se) > 0.3 + 0.15p_T\&\&prob > 0.2\&\&sprob < 0.2$

random at RICH

$|pc3sd\phi| < 3\&\&|pc3sdz| < 3\&\&|emcsd\phi| < 3\&\&|emcsdz| < 3\&\&$
$SN_{PMT} \geq 0\&\&e > 0.3 + 0.15p_T\&\&prob < 0.2$

random on EMC energy

$|pc3sd\phi| < 3\&\&|pc3sdz| < 3\&\&|emcsd\phi| < 3\&\&|emcsdz| < 3\&\&$
$|semcsd\phi| < 4\&\&|semcsdz| < 4\&\&N_{PMT} \geq 0\&\&(e) < 0.3 + 0.15p_T\&\&(e + se) > 0.3 + 0.15p_T\&\&prob < 0.2$

random on EMC *prob*

$|pc3sd\phi| < 3\&\&|pc3sdz| < 3\&\&|emcsd\phi| < 3\&\&|emcsdz| < 3\&\&$
$|semcsd\phi| < 4\&\&|semcsdz| < 4\&\&N_{PMT} \geq 0\&\&e > 0.3+0.15p_T\&\&prob > 0.2\&\&sprob < 0.2$

where $pc3sd\phi(pc3sdz)$ are track matching along ϕ(z) direction in number of standard deviations(σ) at PC3. Similarly, $emcsd\phi(emcsdz)$ are track matching along ϕ(z) direction in number of σs at EMCal. N_{PMT} is the number of associated PMT's at RICH, e ($prob$) are the associated EMCal cluster energy and $prob$ value. The corresponding randomly associated (calculated via flip and slide method [4]) variables are $spc3sd\phi$, $spc3sdz$, $semcsd\phi$,$semcsdz$, SN_{PMT}, se and $sprob$. Note that due to the additive nature of the cluster energy at EMCal, one have to add up the randomly associated energy and original energy. This is definitely an overestimation, because an EMCal cluster requires a local maximum, which typically leads to the cluster energy less than the sum. [3]

The amount of random background for each variable is $f(p_T) \times \epsilon_{ran}$, where

- $f(p_T)$ is the track dN/dp_T before applying this cut.
- ϵ_{ran} is the random association probability for passing the cut on the variable.

[3]The best way to study cluster overlapping effect is through embedding.

Because of this, the amount of random background depends on the cuts applied on other variables. For example, the random association probability at PC3 is about 2% in Minimum Bias $Au-Au$ collisions. However, the spectra $f(p_T)$ with EMCal energy cut is greatly reduced comparing with the one before the energy cut, thus the total random background at PC3 is also reduced if we require the energy cut. This also implies that, if the cut on one variable rejects most of the background(for example the cut on EMCal energy), then the random rejection on this variable can become important. For example, when the energy cut has a large rejection factor, for clusters with energy e below the energy cut, their random overlapped cluster energy, $e+se$, can pass the energy cut with a probability comparable to the signal.

In our study, the full random background is taken to be simply the sum of the random backgrounds for each variable. The background estimated this way is an upper limit, because the different random contributions can overlap with each other. Fig. 25 shows the occupancy study for 50-92% $Au-Au$ centrality. The average N_{coll} weighted by event multiplicity is about 40(corresponds to centrality of 60%). Fig. 25a compares the total pion signal(open circles) with the total random background(close circles). The different contributions to this background are shown in Fig. 25b. The random association to RICH (open diamonds) dominates at $p_T < 6$ GeV/c. At $p_T > 6$ GeV/c region, the random background on energy(filled star) and $prob$(cross) cut also contributes. In the full p_T range, the random association of the matching to PC3 and EMCal, shown by the open boxes, is negligible. The total random background level, shown in Fig. 25b, is about 6-7% level, and does not depends on p_T at $p_T > 5$ GeV/c. In Fig. 26, we show the occupancy study for 60-92% $Au-Au$ centrality, which has a mean N_{coll} comparable to that in 0-20% $d-Au$ collisions. The estimated background is still low $\lesssim 5\%$. In particular, we see that the random background passing cluster energy and cluster shape cut is small($< 1\%$).

In addition to the centrality dependence of the random background, we also need to take into account the centrality dependence of the tracking efficiency. Based on the embedding study for RUN2 $Au-Au$ collisions, the correction for peripheral $Au-Au$ is 1 ± 0.02 [13], which can be used as an upper limited on the centrality dependence.

4.2 Random benefit

Since we use Level-1 triggered data, any possible centrality dependent trigger efficiency, $\epsilon_{trig}(p_T, N_{part})$, and trigger bias, $bias(p_T, N_{part})$ must be taken into account. It is possible that the triggered events containing high p_T pions are actually fired by other particles, we call this random benefit. $bias(p_T, N_{part})$ refers specifically the fraction of such events that are actually fired by the pions. Centrality dependent of the $bias(p_T, N_{part})$ arises when the random benefit effect is centrality dependent. In the case of electron Level-1 trigger, the trigger condition is approximately $npe \geq 3 \&\& E_{2\times 2} > 0.7$ GeV. It could happen that an event containing a high p_T pion is fired by an low energy electron since it's shower profile is more localized and can be easily contained in 2×2 towers. If we use the notation for the track by track high p_T pion trigger efficiency defined in Eq1, $\epsilon_1(p_T, N_{part})$, then the effective trigger efficiency is larger due to the random benefit,

$$\epsilon_{trig}(p_T, N_{part}) = \epsilon_1(p_T, N_{part})/b(p_T, N_{part}). \quad (2)$$

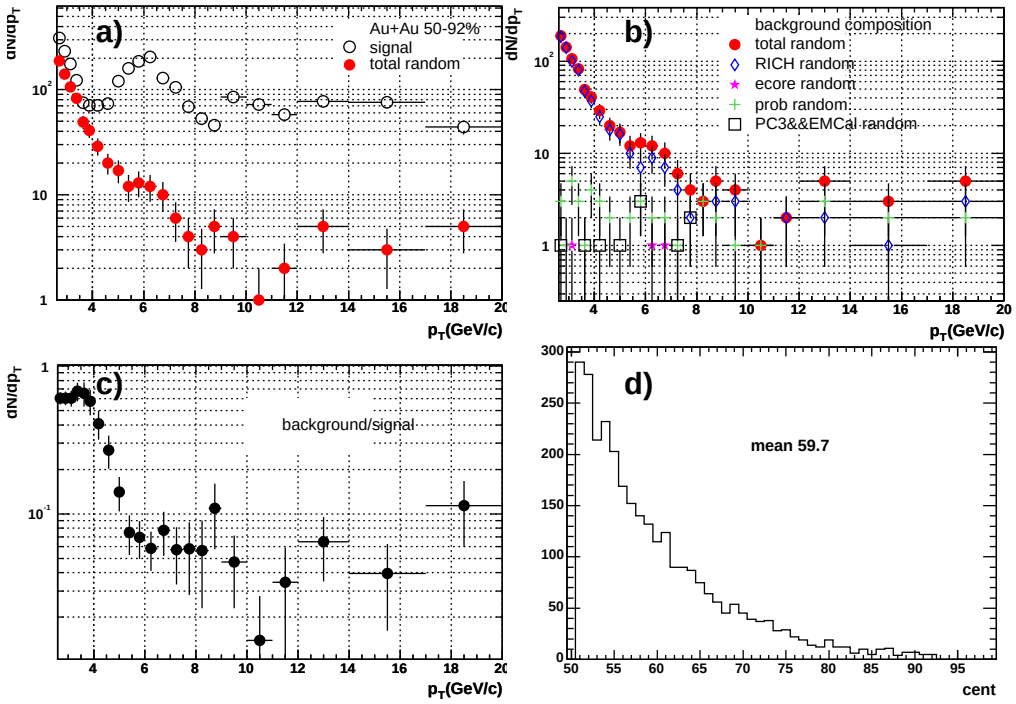

Figure 25: a) Signal and total random background as function of p_T for 50-92% $Au-Au$ collisions. b) Random background decomposed into different contributions. c) Background/signal level. d) pion statistics vs centrality.

$bias(p_T, cent)$ can be directly studied from the data. By matching the Level-1 trigger tiles firing the trigger with the RICH PMT and EMCal towers associated with the charged high p_T pion reconstructed offline [4], we can figure out whether the given charged pion actually fired the Level-1 trigger. The result of this study is presented in Fig. 27. As one can see, the fraction of charged high p_T pions from Electron trigger events that actually fired the events is more than 90%. This value increases to above 95% at $p_T > 8$ GeV/c. The central value is systematically larger than peripheral value by about 2-5%. One can also notice this fraction decreases towards lower p_T for all centralities. This decrease reflects the decrease in trigger efficiency and the increase in random benefit. To reduce the systematic uncertainties on the R_{cp}, we only include those events where the charged pions are the triggers themselves, in other words, we do not include random benefit in our analysis.

4.3 Electron-Trigger trigger efficiency for high p_T pions

In principle, one should be able to evaluate the trigger efficiency, ϵ_{trig}, and it's centrality dependence directly from minimum bias data. Combining with the knowledge on random benefit, one can then obtain the track by track trigger efficiency ϵ_1 and it's centrality dependence. Fig. 28 shows the Electron trigger and Photon trigger efficiencies as evaluated

[4] We use XieWei's smTileModule class to do the matching.

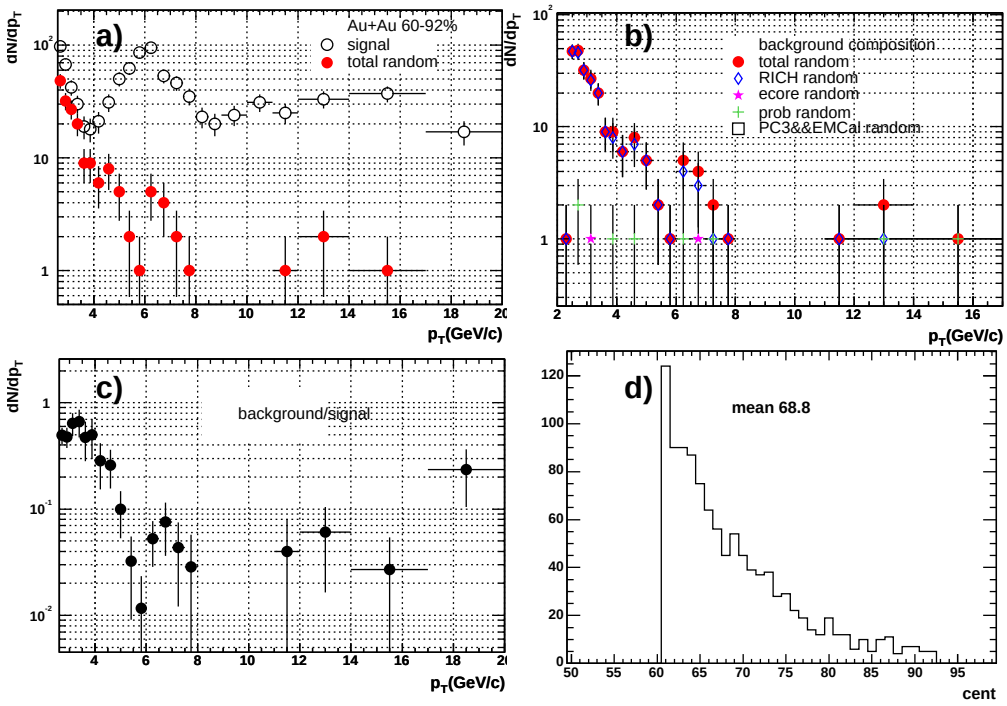

Figure 26: a) Signal and random background as function of p_T for 60-92% $Au-Au$ collisions. b) Random background decomposed into different contributions. c) Background/signal level. d) pion statistics vs centrality.

from minimum bias data. The Photon trigger under consideration contains all three gamma triggers. Both triggers can selects high p_T pions, and Photon trigger have a somewhat higher efficiency than that for Electron trigger. However, in our current analysis, we do not use Photon trigger to select high p_T pions because it is more complicated. There are three Level-1 photon triggers, and the trigger threshold setting were less stable comparing to that for Electron trigger.

Based on the limited statistics of minimum bias events, the track by track trigger efficiency for pion candidates passing offline cut, ϵ_1 is about 40-80% from 5-16 GeV/c. However, one can't not derive ϵ_1 accurately enough to study it's centrality dependence. So we have to find an independent method.

The reason for the centrality dependence of ϵ_1 is that in central $d-Au$ collisions, the overlap of the clusters effectively shift up the cluster energy and thus have a slightly larger chance to fire the trigger than in peripheral collisions. However, most of this bias has been included in random background study in section.4.1 and the bias found there is small. In fact, the change in effective 2×2 energy threshold due to cluster merging should reflect itself as an increase in the total cluster energy. In Fig. 25 and Fig. 26, we have shown that the offline occupancy effect in changing the cluster energy is very small, which should also be the case for 2×2 tower energy in the Level-1 trigger.

The other fact one should remember is, we uses both *prob* and energy cut, and both cuts are very effective in removing the conversion backgrounds. In $5 < p_T < 8$ GeV/c range, after

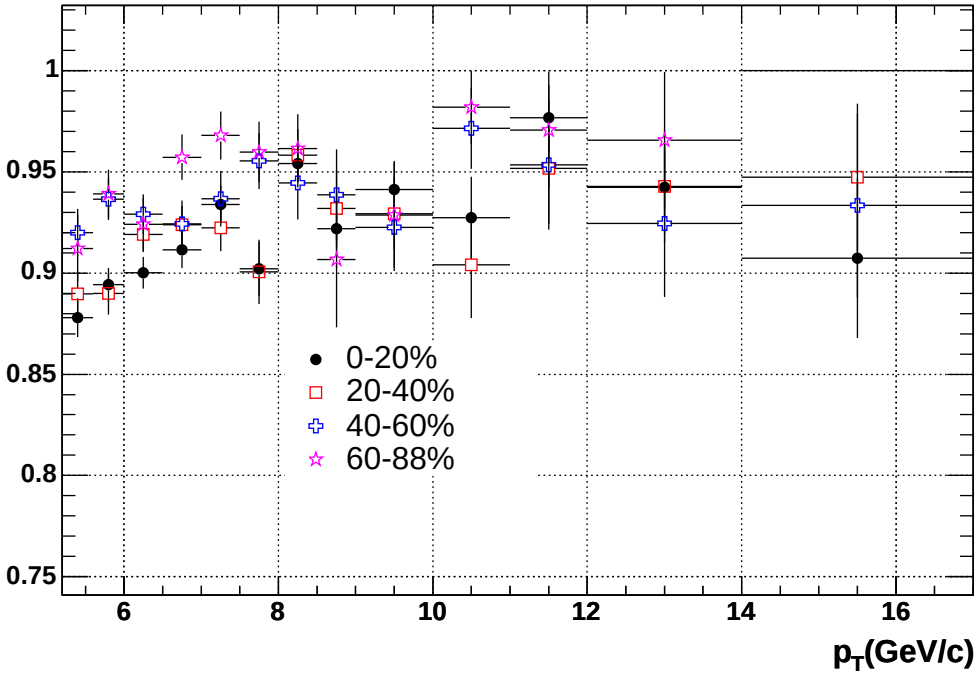

Figure 27: The fraction of pions in Electron triggered events that actually fired that events. Results are presented for four centrality classes.

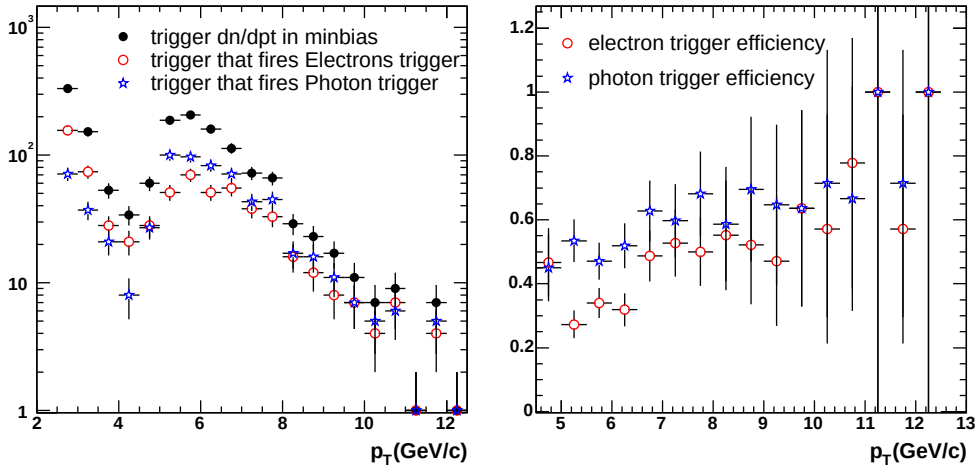

Figure 28: a) All high p_T pion candidates in offline(solid marker), those fired Electron trigger(open circle) and those fired Photon triggers (open star) for minimum bias collisions. b) The corresponding efficiencies for Electron trigger (open circle) and Photon triggers(open star), the two histograms were obtained by dividing the lower two histograms with the upper histograms in the Left panel.

applying the *prob* cut, the change in the pion yield by applying energy cut is only on 20% level. The occupancy effect on varying the energy threshold should only be considered for

this 20%.

To test the scale of the problem, let's assume the average threshold is increased by 0.1 GeV for central collisions. Fig. 29 shows the relative pions efficiency with 0.1 GeV increase on either total energy or it's ecore energy. The histogram with solid and open symbols were evaluated by decreasing the cut on the EMCal e and $ecore$ by 0.1 GeV, respectively. This leads to a 5% p_T independent increase in pion identification efficiency. Since it is unlikely that the Level-1 threshold would change by more than 0.1 GeV due to occupancy effect, the 5% should be the upper limit on the centrality dependence of the ϵ_1.

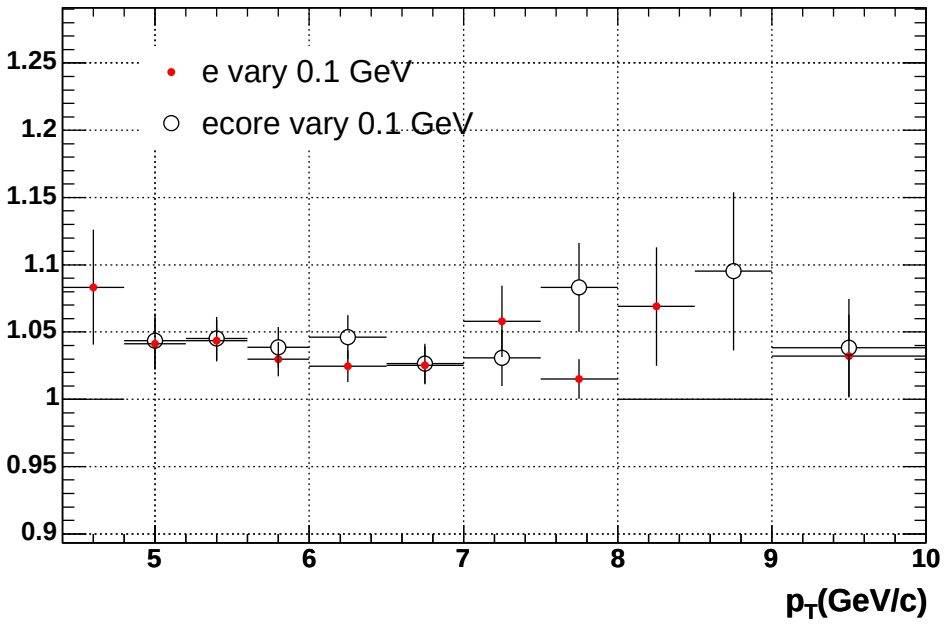

Figure 29: The relative pion trigger efficiency by increasing average e or ecore is increased by 0.1 GeV.

4.4 Systematic errors

In table. 4, we summarize all the systematic errors on R_{cp} that we have discussed in this section. We know that the offline pion efficiency, ϵ_{off} is about 20%, based on earlier study done by Federica [1] and RUN2 charged hadron analysis [4]. Since we also know the Level-1 trigger efficiency is 40-80%, the over all efficiency for pion is at least 8-16%. This is a very conservative lower limit, because pions that pass Level-1 trigger should by definition has large energy deposition in EMCal and thus should have very high probability to be identified as a pion in offline. Thus we believe that the actually efficiency should be very close to 20%.

centrality	minbias/60-88	0-20/60-88	20-40/60-88	40-60/60-88
N_{coll}	7%	11%	6.25%	4.8%
bbc trig bias	1%	1%	1%	1%
Error on the total sampled evts	2%			
Single track bias	±4%			
Offline random background	±5%			
Offline cent dependent efficiency	±5%			

Table 4: A list of the systematic errors on charged pion R_{cp}. The uncertainty on N_{coll} is from analysis note 233[6].

	minbias(M)	0-20%(M)	20-40%(M)	40-60%(M)	60-88%(M)
set1(all data)	4315.2	976	965.5	967.1	1406.8
set2($run > 76284 run! = 78402$)	3050.3	689.9	682.6	683.6	994.5
set3(all peculiar runs)	1265	286.1	283	283.5	412.4

Table 5: The statistics for three run groups.

4.5 Results

The standard tracks cuts are:

- $quality == 31 || quality == 63$
- $fabs(pc3sdz) < 3 \&\& fabs(pc3sd\phi) < 3 \&\& fabs(emcsdz) < 3 \&\& fabs(emcsd\phi) < 3$
- $N_{PMT} \geq 0$
- $e > 0.3 + 0.15 p_T \&\& prob < 0.2$

To check the sensitivity of our results on different data sets, we produces the raw spectra and R_{cp} for several run groups listed in Table.5. Set2 excluded convertor runs(75364-76285), runs with large proton antiproton mass split, which indicates a beam shift(72500-75000, see Wolf's analysis note), runs where ERT trigger are not stable (run< 71723), runs with peculiar number of events per triggered pion according Fig. 6 (76274,74660 and 78402). There are only a few runs before 76284 ([71723-72500]), we also exclude them in the good run. Set3 uses all runs excluded in Set2. The charged pion R_{cp} for CNT_Electron for Set1, Set2 and Set3 are shown in Fig. 30-Fig. 32. The systematic errors are from Tab. 4.

To illustrate the variation of the R_{cp} values on the choice of datasets. In Fig. 33, we show the ratio of the spectra from set2 and set3 in 0-20% central collisions(normalized by number of events). The set2 is about $6.5 \pm 3\%$ higher than set3. But no apparent p_T dependence is seen. Based on this, we concluded that we can uses all the statistics for R_{cp}.

Finally, we can compare with the R_{cp} measured in low p_T identified charged pions from Felix [14] and also R_{cp} for neutral pions in intermediate p_T from Christian [15]. The data points for charged pion are summarized in Table.6-8.

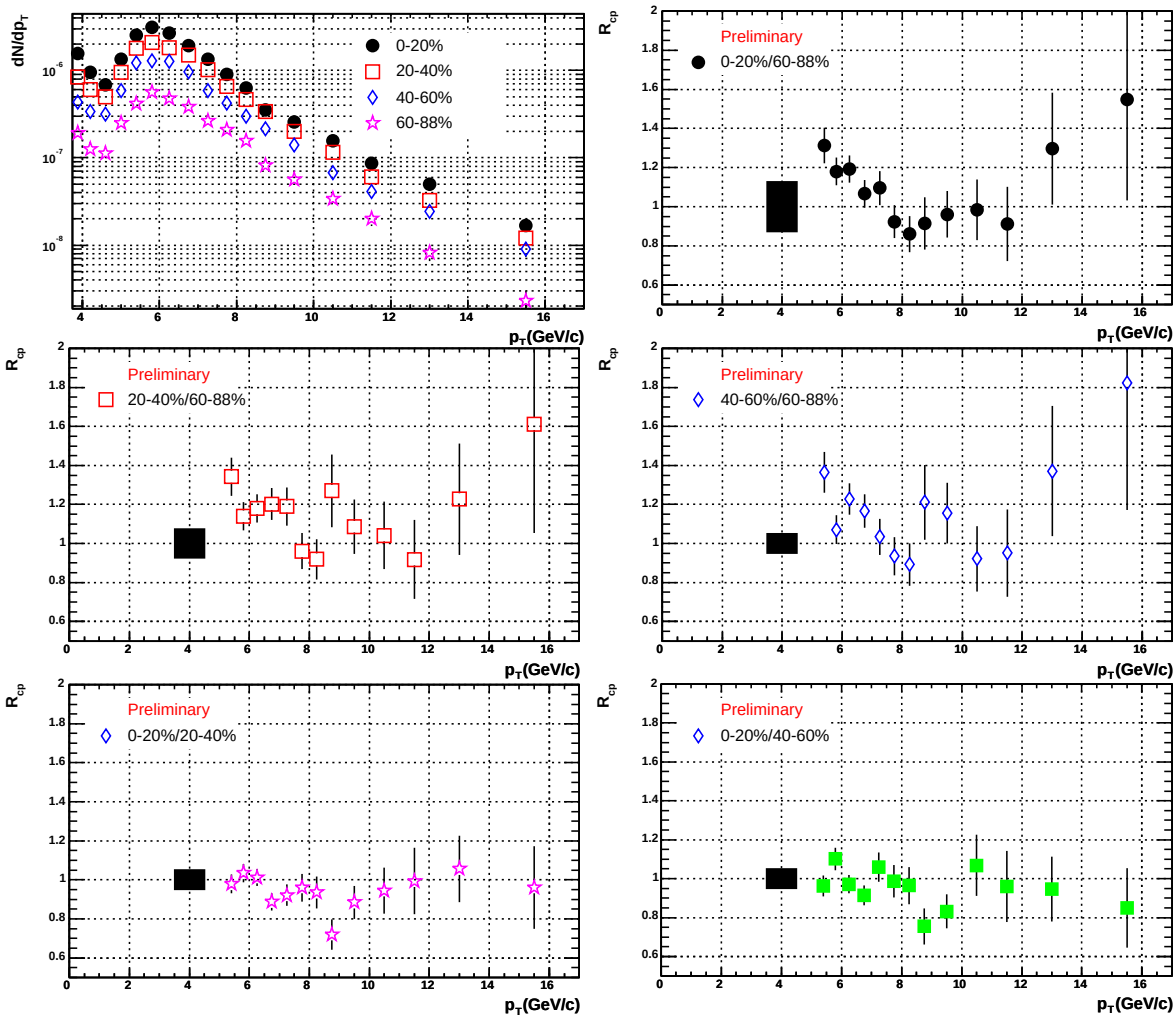

Figure 30: Raw spectra and R_{cp} calculated from electron triggered events, set1

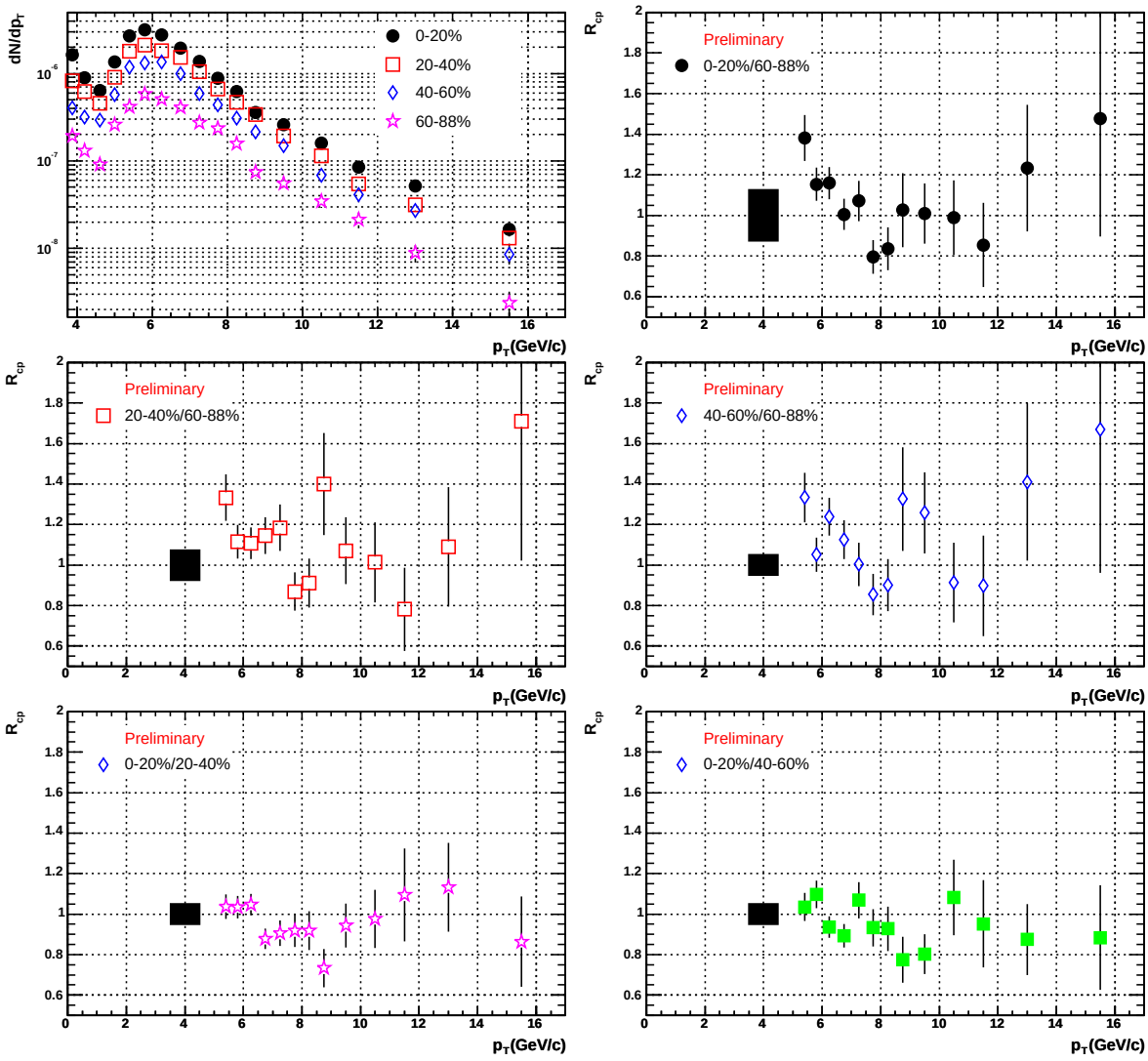

Figure 31: Raw spectra and R_{cp} calculated from electron triggered events, set2

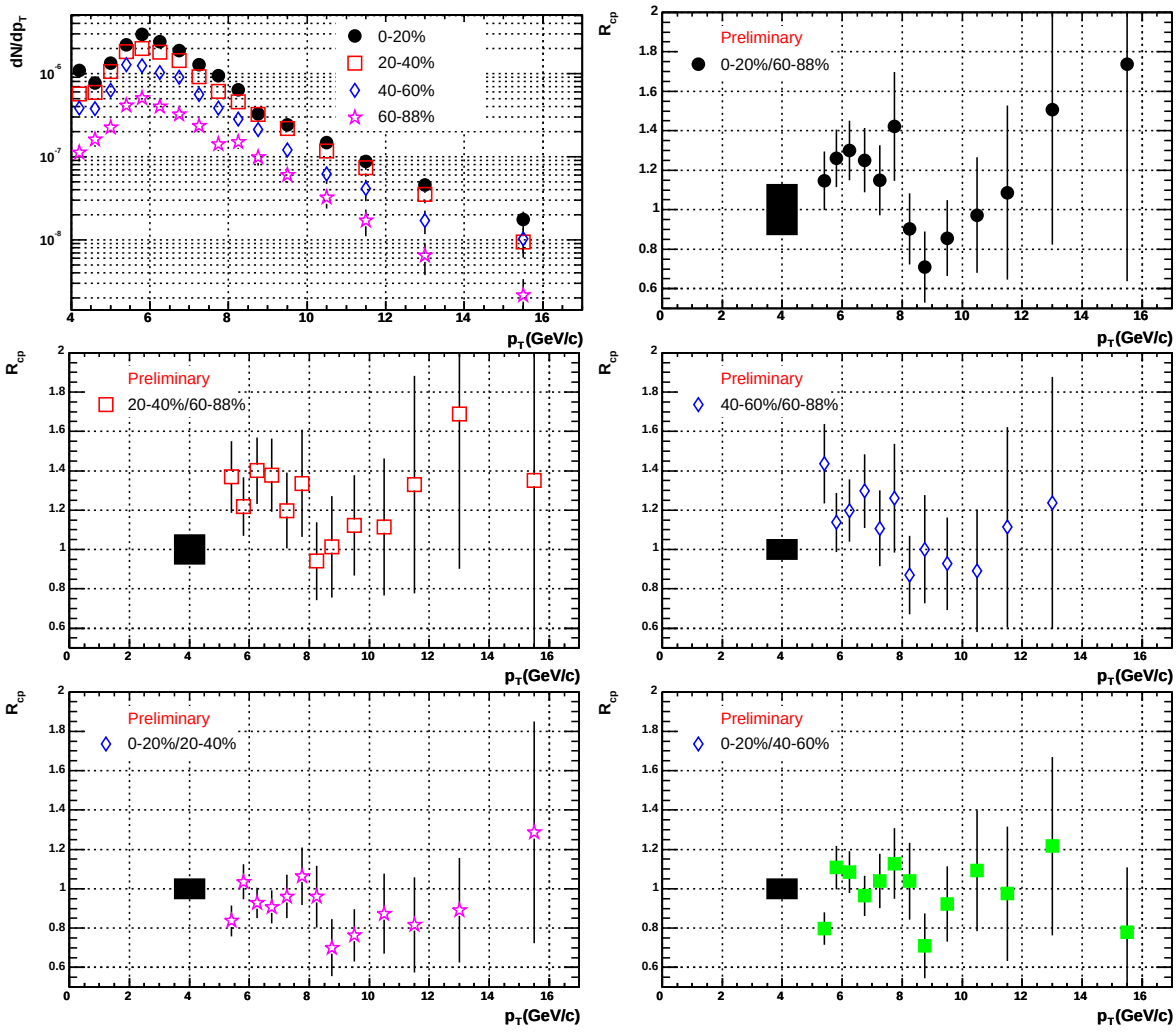

Figure 32: Raw spectra and R_{cp} calculated from electron triggered events, set3

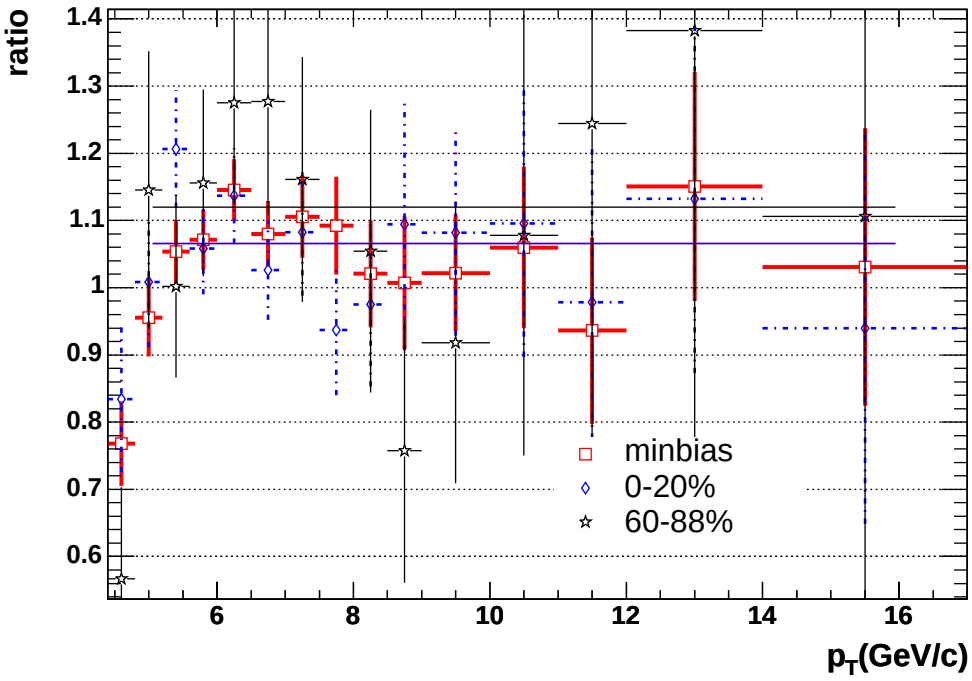

Figure 33: Ratio of set2 yield to set3 yield per event for minbias, 0-20% and 60-88% $d-Au$ collisions.

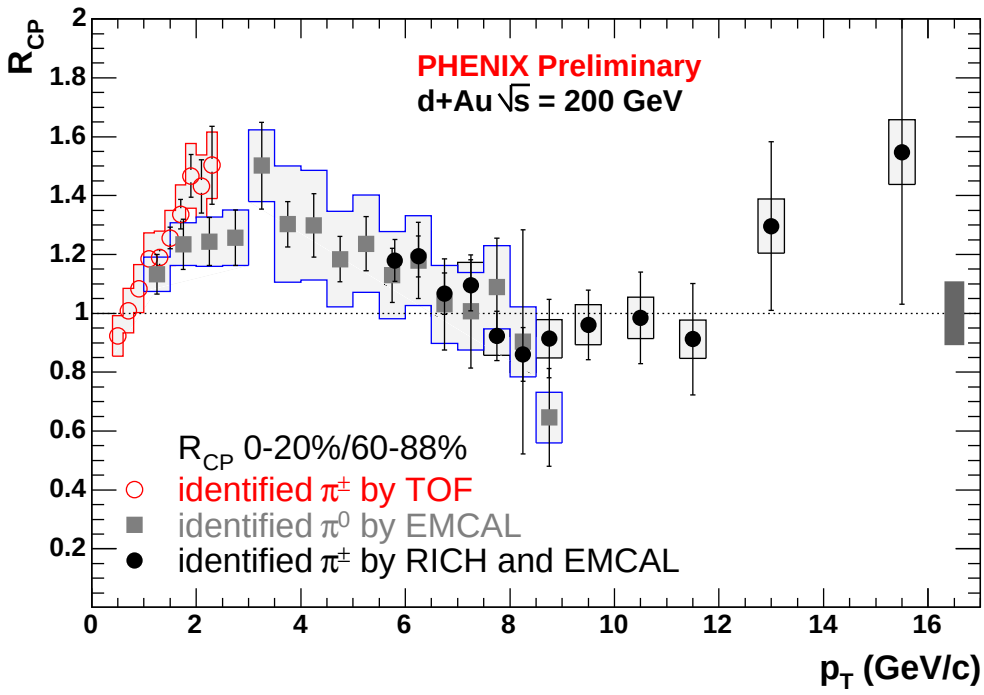

Figure 34: Central(0-20%) to peripheral(60-88%) ratio for three independent pion measurement.

p_T (GeV/c)	R_{cp}	stat error	sys error(%)	error on N_{coll}(%)
5.8	1.17959	0.0710327	7.13	10.87
6.25	1.19363	0.0696672	7.13	10.87
6.75	1.06621	0.0701832	7.13	10.87
7.25	1.09556	0.0869723	7.13	10.87
7.75	0.923057	0.0840523	7.13	10.87
8.25	0.86023	0.0915321	7.13	10.87
8.75	0.914073	0.133193	7.13	10.87
9.5	0.961291	0.118232	7.13	10.87
10.5	0.984455	0.155825	7.13	10.87
11.5	0.912068	0.189471	7.13	10.87
13	1.29627	0.28627	7.13	10.87
15.5	1.54775	0.516396	7.13	10.87

Table 6: R_{cp} for central(0-20%) to peripheral(60-88%).

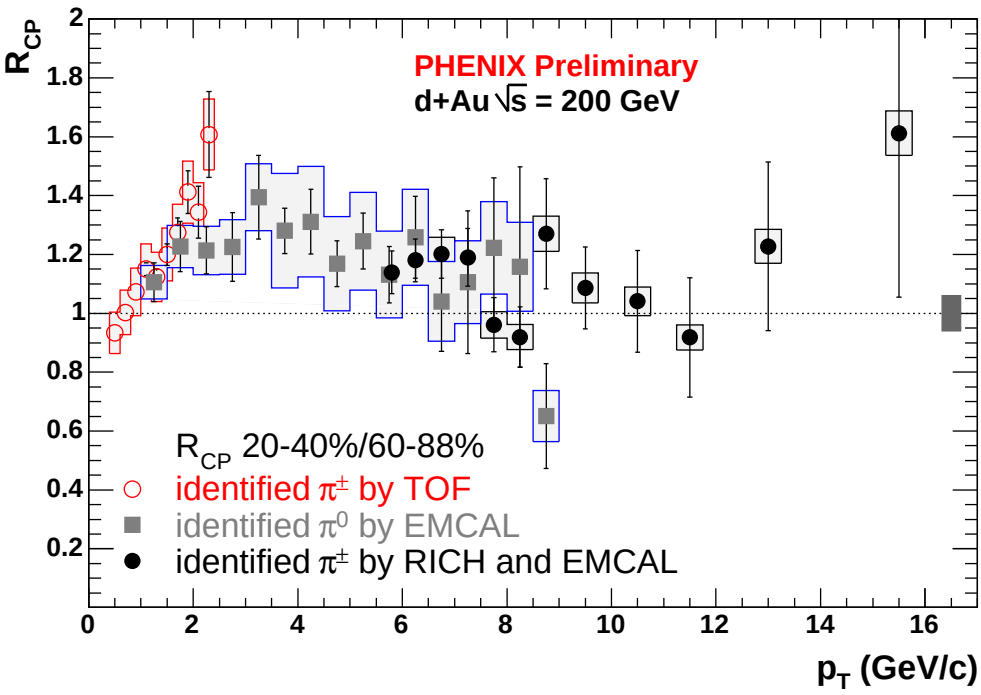

Figure 35: Central(20-40%) to peripheral(60-88%) ratio for three independent pion measurement.

p_T (GeV/c)	R_{cp}	stat error	sys error(%)	error on N_{coll}(%)
5.8	1.13935	0.0724758	4.67	6.25
6.25	1.18013	0.0724702	4.67	6.25
6.75	1.20178	0.0819096	4.67	6.25
7.25	1.18999	0.0982831	4.67	6.25
7.75	0.961194	0.092188	4.67	6.25
8.25	0.919114	0.102797	4.67	6.25
8.75	1.27023	0.186337	4.67	6.25
9.5	1.08623	0.138649	4.67	6.25
10.5	1.04121	0.172751	4.67	6.25
11.5	0.918093	0.202171	4.67	6.25
13	1.22737	0.286097	4.67	6.25
15.5	1.6117	0.557099	4.67	6.25

Table 7: R_{cp} for central(20-40%) to peripheral(60-88%).

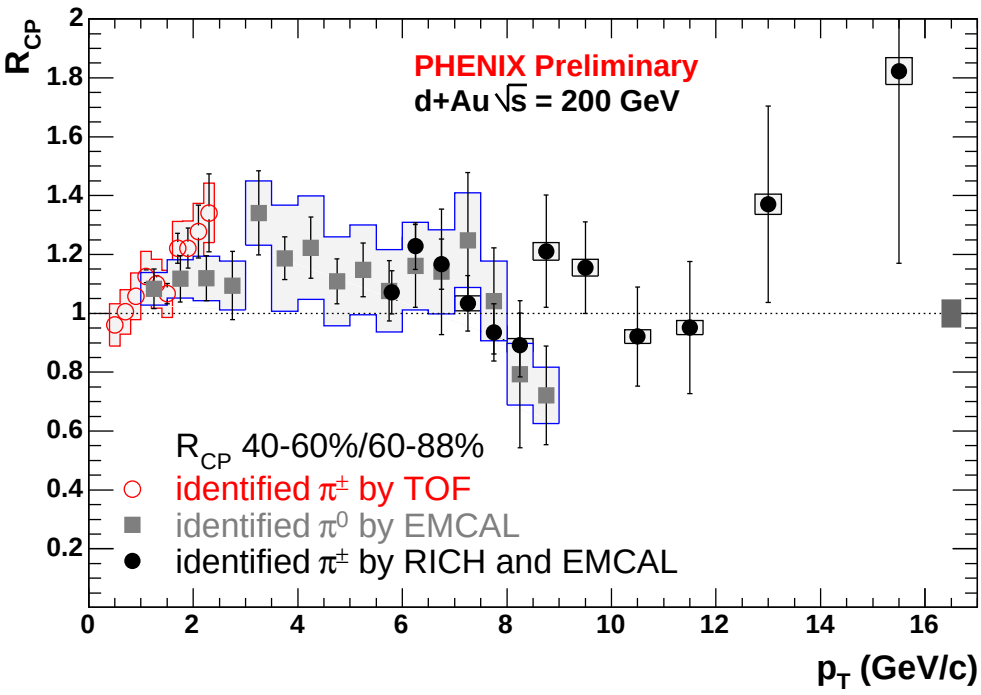

Figure 36: Central(40-60%) to peripheral(60-88%) ratio for three independent pion measurement.

p_T (GeV/c)	R_{cp}	stat error	sys error(%)	error on N_{coll}(%)
5.8	1.07107	0.0737628	2.5	4.8
6.25	1.2283	0.0799193	2.5	4.8
6.75	1.16708	0.0853405	2.5	4.8
7.25	1.03377	0.0937324	2.5	4.8
7.75	0.934794	0.0971861	2.5	4.8
8.25	0.892159	0.108447	2.5	4.8
8.75	1.21079	0.190747	2.5	4.8
9.5	1.15495	0.156042	2.5	4.8
10.5	0.92121	0.168468	2.5	4.8
11.5	0.951287	0.224391	2.5	4.8
13	1.37071	0.333775	2.5	4.8
15.5	1.82242	0.651872	2.5	4.8

Table 8: R_{cp} for central(40-60%) to peripheral(60-88%).

References

[1] F. Messer and J.Jia, High momentum identified pions using the RICH.

[2] F. Bauer, F. Kajihara and K. Okada, Analysis note 228, EMCal/RICH trigger performance in Run 3.

[3] J. Jia, A. Drees, B.A. Cole, V.S. Pantuev, B.V. Jacak, T.K. Hemmick, Study on Charged High pT Background in PHENIX

[4] J. Jia, Ph.D. thesis, http://www.phenix.bnl.gov/WWW/publish/jjia/thesis/thesis.pdf.

[5] A.Drees, T.Hemmick, B.Jacak, J.Jia, S.Leckey, A.Milov, M.Reuter, A.Sickles, R.Soltz, Centrality determination and pT centrality dependency in d-Au collisions.

[6] S. Leckey, B. Jacak, S. Milov, Centrality Dependence of Charged Spectra in pA and nA.

[7] Sasha Besilevsiky's study of PbSc responds with test beam data.

[8] L. Aphecetche, *et.al*, Analysis note 144, Year-2 Inclusive Photon Analysis in PbSc for QM02 and Systematic Errors

[9] PPG14.

[10] PPG23.

[11] PPG28.

[12] PPG29.

[13] https://www.phenix.bnl.gov/phenix/WWW/p/lists/phenix-hard-l/msg03051.html.

[14] Felix Matathias, QuarkMatter proceedings, nucl-ex/0403029.

[15] Christian Klein-Boesing, QuarkMatter proceedings, nucl-ex/0403024.